RSC Advances

ROYAL SOCIETY OF CHEMISTRY

www.rsc.org/advances

Graphical abstract

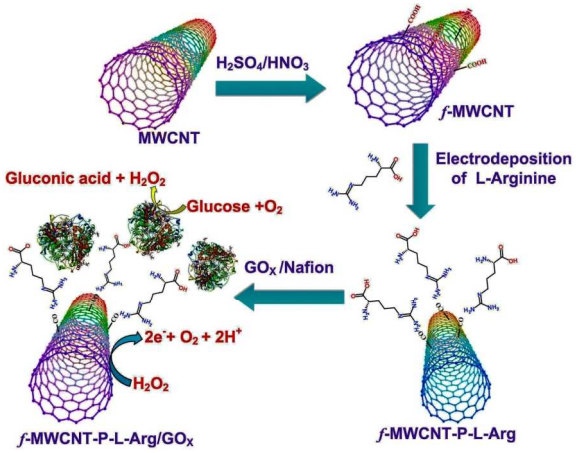

Schematic diagram of the preparation of GOx/P-L-Arg/*f*-MWCNTs/GCE modified electrodes for glucose biosensors.

Direct electrochemistry and electrocatalysis of glucose oxidase based poly (L-arginine)-multi-walled carbon nanotubes

A.T. Ezhil Vilian, Shen-Ming Chen*

Department of Chemical Engineering and Biotechnology, National Taipei University of Technology, No.1, Section 3, Chung-Hsiao East Road , Taipei 106, Taiwan (R.O.C).

*Corresponding author. Fax: +886 2270 25238; Tel: +886 2270 17147, E-mail: smchen78@ms15.hinet.net

Abstract

This paper reports a simple and fast approach for the construction of a novel glucose biosensor based on the electro polymerization of a Poly-L-arginine film (P-L-Arg) onto functionalized multiwalled carbon nanotubes (*f*-MWCNTs) /glassy carbon electrode (GCE) via electrostatic attraction with glycoprotein glucose oxidase (GOx). The morphological and electrochemical properties of the prepared composite were studied by scanning electron microscopy, electrochemical impedance spectroscopy, cyclic voltammetry, X-ray photoelectron spectroscopy and Fourier transform infrared spectroscopy. The prepared GOx-/P-L-Arg/*f*-MWCNTs film modified electrode shows a well defined reversible redox couple at a formal potential of -0.45 V (vs. AgCl) with significantly enhanced peak currents corresponding to the direct electrochemistry of the GOx. The direct electron transfer process is a surface-controlled electrode process with a high heterogeneous electron transfer rate constant (k_s) of 5.16 s^{-1}. Moreover, this modified electrode was demonstrated to be an efficient glucose biosensor by means of the reductive detection of oxygen consumption. The proposed biosensor possesses excellent analytical parameters for a wide linear range of glucose from 4.0 μM to 6 mM (a correlation coefficient of R^2=0.9918) with a 5 s response time. The sensitivity of the biosensor is found to be 48.86 μA cm^{-2} mM^{-1}, its experimental detection limit is 0.1μM (S/N = 3), the apparent Km is calculated to be 2.2 mM and it also exhibits good storage stability for 25 days. The novel biosensor developed in this study exhibits a fast response, high stability and very good reproducibility.

Keywords: Glucose oxidase, Poly-L-arginine, functionalized multiwalled carbon nanotubes, direct electrochemistry, biosensor.

1. Introduction

Over the past few years, the direct electrochemistry of redox enzymes/proteins by biosensors has been investigated extensively. [1] Determination of glucose concentration requires great sensitivity and accuracy and is of extreme importance in the fields of food industry, biology, environmental protection, and clinical analysis. [2, 3] High levels of blood glucose with a concentration ranging between 80 and 120 mg/dL (4.4-6.6 mmol L^{-1}) can lead to serious complications, including higher risk of heart disease, kidney failure, and blindness from diabetes mellitus, which is a metabolic disease. [4,5] Up to now, several analytical methods have been proposed for the determination of glucose, including capillary zone electrophoresis, [6] Fourier transform infrared spectroscopy,[7] fluorescence spectroscopy, [8,9] and surface plasmon resonance, [10]and electrochemical methods. [11] However, these techniques have certain drawbacks such as being labor-intensive, time-consuming sample preparation and requiring expert handling and expensive instruments. Electrochemical techniques have led to the development of highly sensitive, reliable, simple instrumentation that is low cost, and exceptionally compatible with miniaturization. [12] Research has mainly focused on the development of enzyme biosensors and furthering the development of amperometric glucose sensor studies, focusing on the glucose oxidase catalyzed conversion of glucose to gluconolactone. [13]

Homodimers of GOx having a molecular weight of about 150-180 kDa and containing flavine adenine dinucleotide (FAD) cofactors as the redox center, are deeply embedded within a protein shell, making them inaccessible for direct communication with the electrode surface. [14,15] The challenge in the development of electrochemical glucose biosensors is to achieve DET between the GOx and the electrode surfaces. [16] GOx enzyme immobilization is thus a key factor in the preparation of glucose biosensors and various modified electrodes have been proposed in

the literature, such as those comprised of nanomaterials, Au nanoparticles, [17]carbon nanotubes (CNTs), [18] graphene, [19, 20] nickel oxide nanoparticles, [21] molecular wires, [22] and polymer films. [23]

In recent years, CNTs have received great attention as nanomaterials for the fabrication of electronic devices because of its extraordinary physical and electrical properties such as high tensile strength, highly elastic modules, and high thermal and electrical conductivity.[24] Owing to its excellent ability to provide a desirable microenvironment and facilitate the DET between the redox sites of an enzyme and the electrode surface CNTs have been used as the electrode material in many electrochemical reactions. [25] As an electrode material, CNTs provide a novel platform for fabricating chemical sensors or biosensors, and can be used to promote electron-transfer between the electroactive species and the electrode. [26] To make them useful for such applications, MWCNTs are activated by an oxidative process which acts to insert functional groups on the sidewalls. [27] A variety of methods have been used for the deliberate incorporation of surface oxygen into CNTs, chief among these being wet chemical oxidation, plasma treatment and rational functionalization strategies involving synthetic organic chemistry. [28] Among the various treatment methods, the wet chemical oxidation process is recognized as being one of the most efficient processes for MWCNT dispersion and surface activation. The oxidation of MWCNTs is widely performed by refluxing with oxidizing agents such as H_2SO_4, HNO_3, H_2SO_4/HNO_3, $KMnO_4$, $KMnO_4/H_2SO_4$, HNO_3/H_2O_2 and H_2O_2. These tend to be the most prevalent because they are easy to implement in laboratory and industrial settings. [29] It has been observed that during the oxidation process a variety of functional groups such as carboxylic (-COOH), carbonyl (-C=O), and hydroxyl (-OH) groups form on the surface of the MWCNTs. [30] These functional groups promote MWCNTs' chemical reactivity. This in turn, enhances the dispersability of the MWCNTs in aqueous solutions and organic solvents and thus can be

directly used for composite fabrication. Some studies have attempted to investigate the effect of the oxidation time when using a H_2SO_4/HNO_3 mixture on the structure and surface chemistry of MWCNTs. [31]

Recent results indicate a further enhancement of performance for carbon nanotube/polymer composite supported electrodes over that of individual carbon nanotubes or polymer supported electrodes. [32] However, the introduction of amino groups into the CNTs can improve their solubility in many solvents. More importantly, due to its chemical versatility, the amino group acts as a useful precursor for surface modification of CNTs, reacting with other organic molecules, polymers and biological systems to produce hybrids. [33] In fact, amino-functionalized carbon nanotube-based composites have drawn much attention due to their outstanding properties, such as activity and durability, in various electrochemical reactions derived from their hybrid structures. [34] Therefore, the $-NH_2$ and -COOH groups of amino acids play a key role in the electro-polymerization process on the electrode surface. [35] Owing to the excellent electrocatalytic properties of amino acids, different types of poly amino acids have been prepared by chemical and electrochemical methods for electrochemical sensor applications. [36] However, Poly(L-arginine) has been used for the modification of electrodes and applied for electrochemical determination, owing to its versatility and ease of preparation. This research proposes a new approach to integrating synthetic and biological polymers by exploiting the observation that proteins can be crosslinked via their L-Arginine residues. [37] On the other hand, composite materials combining graphene and polymer have received increased attention due to the synergistic contribution of two or more functional components and many potential applications. [38] However, only a few reports of the application of poly(L-arginine) for the development of modified electrodes have been recognized.Past studies have shown that the L-

Arginine exhibits high biocompatibility, high adsorption ability and the biological activity of redox proteins. [39]

In this study, we describe for the first time the use of layer-by-layer films of P-L-Arg/*f*-MWCNTs with an encapsulation matrix of GOx for the development of an amperometric glucose biosensor. Due to the lack of a mediator, the biosensor can detect glucose at low potentials with no obvious interference. As we know, the amino group forms a base for the incorporation of biomolecules, and which can provide easy accessibility to the substrate for electron transport. P-L-Arg is a biopolymer having wide applications in the medical and food industries for its high biocompatibility, high mechanical strength, easy manipulation, low cost, excellent film-forming ability and good solubility in an acidic medium. The resultant GOx/P-L-Arg/*f*-MWCNTs film modified GCE electrode can catalyze the oxidation of glucose into H_2O_2 and gluconolactone in the presence of O_2 in a solution. The biosensor has a fast response of less than 5 s with a linear range of 4 μM to 6 mM and a detection limit of 0.1μM. Compared to other biosensors reported in the literature, the newly developed biosensor exhibits a fast response, has a low detection limit and high stability, and very good reproducibility. The experimental results show that the P-L-Arg/ *f*-MWCNTs film modified GCE exhibits excellent electrocatalytic activity for the reduction of H_2O_2 and exhibits a wider linear range and lower detection limit toward H_2O_2. The modified electrode has been demonstrated to function as an efficient glucose sensor and moreover the proposed biosensor exhibited excellent electro catalytic properties, is simple, has good stability, sensitivity and is biodegradable. The GOx/P-L-Arg/*f*-MWCNTs multilayer films provide a new electrochemical platform for fabricating protein-modified electrodes.

2. Experimental Procedure

2.1. Reagents

The GOx, from Aspergillus Niger, MWCNT, D-glucose and Nafion (5 weight% solution) used in this study were purchased from Sigma-Aldrich. All the reagents were of analytical grade and used without any further purification. A phosphate buffer solution (PBS) was prepared by mixing stock solutions of NaH_2PO_4 and Na_2HPO_4, then adjusting the pH values by the addition of either 0.1 M HCl or NaOH solutions. The stock solution of GOx was prepared in a 0.05 M PBS with a pH of 6.5 and stored at 4 ºC. A stock solution of D-glucose was prepared and allowed to mutarotate at room temperature for one day before use. All solutions were prepared with double distilled (DD) water obtained from a Milli-Q water system.

2.2. Apparatus

The electrochemical experiments were performed using a CHI405A electrochemical work station. All of the experiments were carried out by a three-electrode system with a modified GCE as the working electrode (area 0.07cm^2), platinum wire as the auxiliary electrode and saturated Ag/AgCl as the reference electrode. EIS were performed in a Zahner impedance analyzer (Zahner Elektrik GmbH & Co. KG, Kronach, Germany). The morphological characterization was carried out using a Hitachi S-3000H scanning electron microscope (SEM) and Energy-dispersive X-ray (EDX) spectra studies were acquired by using HORIBA EMAX X-ACT (Model 51-ADD0009, Sensor + 24V=16 W, resolution at 5.9 keV = 129 eV) respectively. AFM characterization was carried out by Hitachi and CSPM4000, Being Nano-Instruments respectively. Fourier transform infrared (FTIR) spectroscopy was carried out using a Perkin Elmer RXI spectrometer. Amperometric i-t curve studies were carried out using a rotating disk electrode (RDE) with an analytical rotator AFMSRX (PINE instruments, USA) with the CHI

405A model electrochemical workstation. UV-vis absorption spectroscopy measurements were carried out on a Hitachi U-3300 spectrophotometer and X-Ray photoelectron spectroscopy (XPS) was performed using a PHI 5000 Versa Probe equipped with an Al Kalpha X-ray source (1486.6 eV).

2.3. Acid Treatment of MWCNTs

60 ml of 0.4 M HCl aqueous solutions and 0.5 g of crude MWCNTs were mixed and sonicated in a bath for 4 h, after which 60 ml of concentrated H_2SO_4/HNO_3 (3:1) solution was added to the mixture and then stirred for 4 h under reflux. After that, the solution was diluted with 400 ml of DD water under cooling conditions and vacuum-filtered through a 0.22 μm polycarbonate membrane. The obtained functioned MWCNT (*f*-MWCNTs) black color solid was washed repeatedly with DD water until the pH of the filtrate became 7. The as-purified *f*-MWCNTs was dried in an oven in a vacuum for 12 h at 60°C.

2.4. Fabrication of GOx/P-L-Arg/*f*-MWCNTs/GCE

The GCE was polished to a mirror-like surface with 0.05 μm alumina slurries and rinsed with water several times. The GCE was then washed using an ultrasonic treatment in ethanol and water for 5 min, respectively, before being dried at room temperature. The *f*-MWCNTs (1 mg/ml) were dispersed in DMF via sonication for 20 minutes. Additionally an optimal amount of 5μL of the *f*-MWCNTs dispersion was drop-cast onto the pre-cleaned GCE and then dried at room temperature, which served to improve biosensor performance. Higher amounts of *f*-MWCNTs could agglomerate on the electrode surface which would affect the catalytic activity and stability. The modified GCE was rinsed with water to remove loosely adsorbed *f*-MWCNTs. Afterwards, a poly (L-Arg) film was formed through polymerization on the *f*-MWCNTs

modified GCE. The *f*-MWCNTs/GCE was transferred into an electrochemical cell with 10ml of PBS (pH6) containing 10 mM of L-Arg. Polymerization of L-Arg was achieved by performing 10 consecutive cyclic voltammograms in the potential range between -2.0 to +2.5 V (vs. the Ag/AgCl reference electrode) at a scan rate of 100 mVs^{-1}. During the cycling at this high positive potential, the monomer L-Arg was oxidized to form an α-amino free radical which stimulates the polymerization. The positively charged polymerized L-Arg (P-L-Arg) surface was crucial for the immobilization of GOx. The as-prepared P-L-Arg/*f*-MWCNTs/GCE was gently washed with water and dried under ambient conditions. The solution was obtained by dissolving 10mg of GOx in 1 mL of PBS (pH 6.5). It should be noted that at this pH, GOx (pI = 4.5) bears a net negative charge. Thereafter, GOx was mixed together rigorously in a pH 6.5 PBS before been stored in a refrigerator for at least 24 h. A load of 10 mg/ml of GOx (unless otherwise specified) is optimal as is shown by observing the redox peak current response and biosensor activity. 10 µL of GOx were drop-cast onto the surface of P-L-Arg/*f*-MWCNTs/GCE to create the resulting modified electrode which was allowed to dry at ambient temperatures. It should be noted that *f*-MWCNTs have a high specific surface area and the carboxylic acid group functionalized *f*-MWCNTs have an advantage for the formation of positively charged polymerized P-L-Arg surfaces. This P-L-Arg/*f*-MWCNTs electrode material combination offers a useful platform for immobilizing biomolecules to enhance sensor performance, and provides a good interaction between the active site of the GOx and the P-L-Arg/*f*-MWCNTs polymer layer. Finally, 1.0 µL of 0.5% Nafion solution was drop-cast and then dried. The modified GOx/P-L-Arg/*f*-MWCNTs/GCE electrodes were stored in a refrigerator at 4 $^{\circ}$C when not in use. The method used to fabrication of GOx/P-L-Arg/*f*-MWCNTs/GCE electrodes is illustrated in scheme 1.

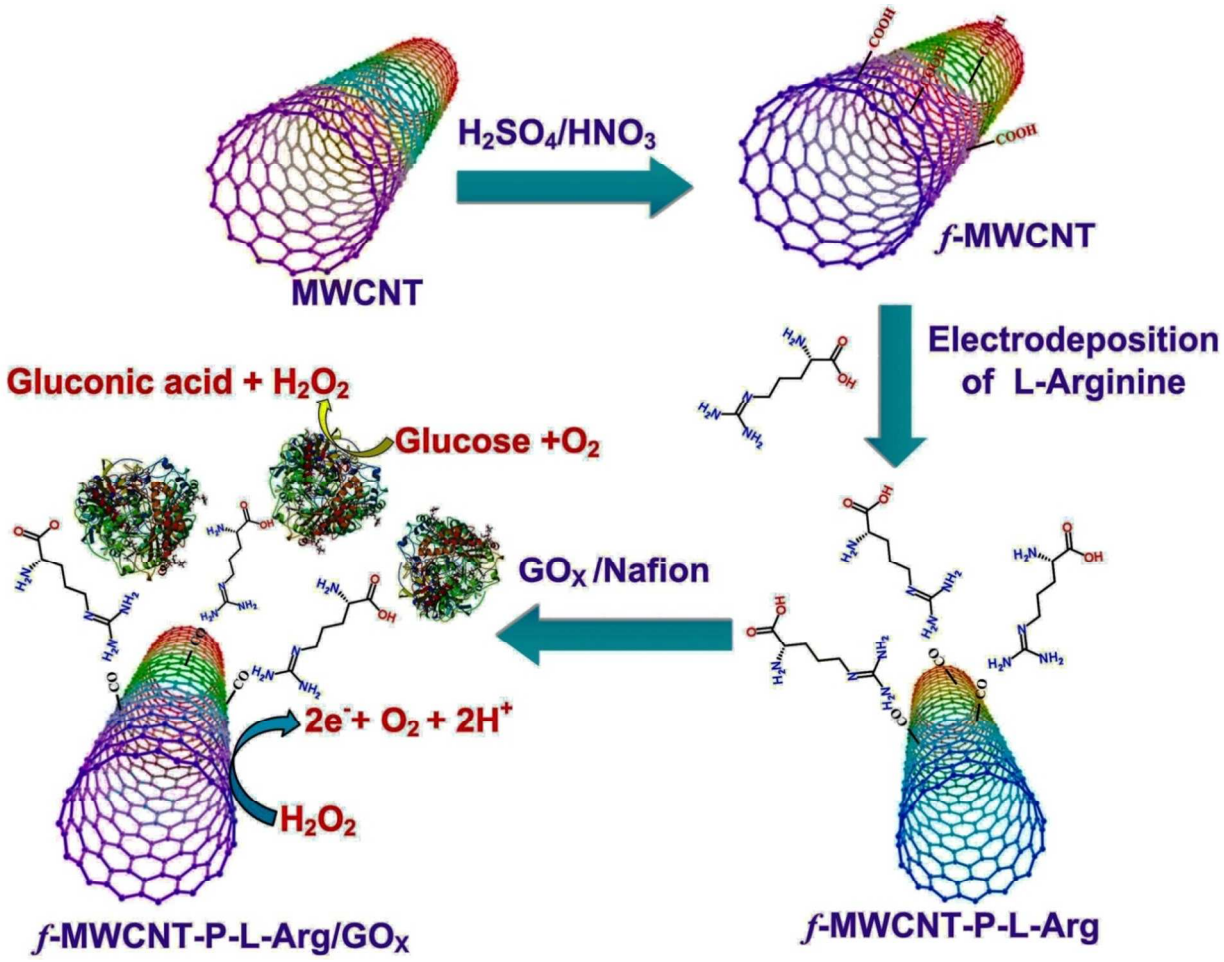

Schematic diagram of the preparation of GOx/P-L-Arg/*f*-MWCNTs/GCE modified electrodes for glucose biosensors.

3. Results and discussion

3.1 . Characterization of GOx/P-L-Arg/*f*-MWCNTs/GCE modified film.

Fig. 1A shows the results of an investigation of the elements on the surface of the P-L-Arg polymer deposited on the *f*-MWCNTs through XPS elementary analysis. Fig. 1 A confirms the presence of nitrogen and an increase of oxygen with respect to MWCNTs, given the reaction with the P-L-Arg. In addition, the XPS results show a slight broadening of the main C 1s and O 1s peaks at 284.79 eV and 532.92 eV in the *f*-MWCNTs (see,Fig. 1B). After that, to provide

clearer evidence of amide bonding between the P-L-Arg on the *f*-MWCNTs, the N 1s peaks of the P-L-Arg on the *f*-MWCNTs were fitted with two component peaks, as shown in Fig. 1C. The lower binding energy peak at 404.1 eV is attributed to the formation of an amide linkage, as the N1s binding energy for amides is expected to be between 399.5 and 405 eV . [40] The higher bonding energy peak at 405.2 eV is assigned to an amine nitrogen ($-CH_2-NH_2$) bond associated with the amine groups on the P-L-Arg of the *f*-MWCNTs surface. These results are in good agreement with reactions taking place between the P-L-Arg on the *f*-MWCNTs as well as with the obtained FT-IR results.

FTIR spectroscopy was used to show the types of functional groups present in the Fig. 1D (a) *f*-MWCNTs, (b) P-L-Arg/*f*-MWCNTs. Fig.1D shows the FTIR spectrum of *f*-MWCNTs (Fig. 1D(a)) with three important characteristic absorption peaks and the band at 1720 cm^{-1} which are attributed to the C=O stretching modes of vibration for the carboxylic acid group, while the band at 1080 cm^{-1} is assigned to O-H deformation vibrations. [41] The above results indicate, the formation of the carboxylic acid group, attached to the top and sidewalls of the MWCNTs. For the P-L-Arg/*f*-MWCNTs modified film (Fig. 1D(b) the L-Arg was polymerized to form a P-L-Arg chain linked through -NH- bonds at the *f*-MWCNTs. The peaks of the C=O bond of the free -COOH groups are at 1294.99 and 1343.93 cm^{-1}, and the -CONH- bonds of MWCNT immobilized on L-Arg is at 1625 cm^{-1}. These results indicate that the possible combination of amino groups in P-L-Arg with carboxyl groups in *f*-$MWCNT_S$ results in the formation of a strong electrostatic attraction. The FTIR spectra of the (a) native GOx, (b) GOx/P-L-Arg and (c) GOx/P-L-Arg/*f*-MWCNTs are shown in Fig. 2C. For native G GOx, (curve a), the intense absorption at 3408 cm^{-1} is assigned to the N-H stretching, and the characteristic peaks observed at 1624 and 1537 cm^{-1} are attributed to amide I (the C=O stretching vibrations of the

peptide bond groups) and II (the N-H in-plane bending and C-N stretching modes of the polypeptide chains) bands of native GOx. [42] The bands for the GOx immobilized at the positively charged surface P-L-Arg are easy to see Fig. 2C (curve b). The spectrum for the GOx/P-L-Arg/*f*-MWCNTs (curve c) also shows two characteristic adsorption bands at 1648 and 1558 cm^{-1}, suggesting that the GOx has been successfully immobilized on the P-L-Arg/*f*-MWCNTs film. The slight shift in the adsorption bands corresponding to amide I and II may come from intermolecular interaction between the GOx and P-L-Arg/*f*-MWCNTs film, which can effectively prevent the leaching of GOx from the P-L-Arg/*f*-MWCNT matrix.

[Fig. 1]

The surface morphologies of the *f*-MWCNTs,and P-L-Arg/*f*-MWCNTs were investigated by images shown in Fig. 1E. As can be observed from the image of Fig. 1E, *f*-MWCNTs resembles the forms of small bundles. The insert image shows the EDX measurements which are also used for quantitative analysis of the presence of the oxygen containing groups on the surface of the carbon nanotubes. The results show the presence of oxygen in the sample in addition to the element carbon. It has been shown that the edge of *f*-MWCNTs yields chemical functional groups, such as -COOH during the acid treatment process. The functional groups make the *f*-MWCNTs more hydrophilic so they are able to interact with the P-L-Arg more easily. This is helpful for increasing the surface loading of the GOx. It can be seen in Fig. 1(F) that the P-L-Arg/*f*-MWCNTs surface is very smooth and homogeneous with an increase in the diameter of the tubes of approximately 2-5 nm, which indicated that the P-L-Arg film covered and linked to the walls of the *f*-MWCNTs. The EDX spectrum in Fig. 1 (F) shows the presence of N, C and O elements in the sample, which further confirms the presence of P-L-Arg on the *f*-MWCNTs surface. From the SEM images of GOx/P-L-Arg/*f*-MWCNTs, it can be seen that GOx

agglomerates are found distributed all over the P-L-Arg/*f*-MWCNTs surface, therefore, the addition of positively charged P-L-Arg can provide a suitable microenvironment for the negatively charged GOx to retain its activity (See Fig.2(A). On ther other hands, The AFM images have shown the surface morphology and film thickness of the *f*-MWCNTs, P-L-Arg/*f*-MWCNTs and GOx/P-L-Arg/*f*-MWCNTs modified electrodes. The AFM images in Fig. S2 reveal a surface characterized by a network of cylindrical features with lengths of several hundreds of nanometers and much smaller in width. These lines represent the segments of the *f*-MWCNTs that approach the surface and confirm a random planar arrangement. After the modification of the *f*-MWCNTs surface with the P-L-Arg film, the polymer film can be clearly observed on the surface to a height of 39.1 nm. The irregularly shaped islands offer a rougher surface than for the *f*-MWCNTs electrode (See Fig.S3). The surface morphology of the L-Arg/*f*-MWCNTs film before and after GOx adsorption can be observed by AFM analysis (See Fig.2B). The AFM images provide information about the roughness of the film. The GOx granules are the sole deposits on the L-Arg/*f*-MWCNTs films. The topographic images indicate that the greater surface roughness, or surface area, of the L-Arg/*f*-MWCNTs film induce much greater GOx adsorption by the film.

[Fig. 2]

The UV-vis absorption spectra of the (a) native GOx, (b) GOx/*f*-MWCNTs, (c) GOx/P-L-Arg and (d) GOx/P-L-Arg/*f*-MWCNTs on ITO electrodes are shown in Fig. 2D. On the GOx (curve a), the two weak peaks at 330 and 402nm can be attributed to the characteristic oxidized form of the flavin group in the protein structure. [43,44] The position and shape of the absorption bands for the GOx/P-L-Arg/*f*-MWCNTs (curve d) are almost the same as those of the native GOx, indicating that the GOx immobilized in P-L-Arg/*f*-MWCNTs film indeed maintains its

native structure. The results may be due to the biocompatibility of the composite materials. P-L-Arg is a biocompatible hydrophilic biopolymer and the *f*-MWCNTs have shown good biocompatible ability to keep the activity of enzymes. Thus the native structure of the GOx can be retained in the P-L-Arg/*f*-MWCNTs composite.

EIS is an important technique for monitoring the changes in the electrical properties of modified electrodes. The Nyquist plot displays two kinds of regions, a semicircular higher frequency region, which corresponds to the electron-transfer resistance (R_{et}) and another linear region at lower frequencies corresponding to the diffusion process. Fig. 3A illustrates the real and imaginary parts of the EIS as represented by the Nyquist plots (Z_{im} vs. Z_{re}) for: (a) P-L-Arg/*f*-MWCNTs/GCE; (b) P-L-Arg/GCE electrode; (c) Bare GCE electrode; (d) GOx/P-L-Arg/*f*-MWCNTs/GCE electrode; (e) GOx/P-L-Arg/GCE electrode; and (f) GOx/GCE electrode in a pH 6.5 PBS solution containing 5 mM $Fe(CN)_6^{3-/4-}$. The inset to Fig. 3A represents the electron transfer resistance (R_{et}) of the bare GCE (c) which exhibits a to be 1040 Ω. The GCE was electro polymerized with P-L-Arg for 10 cycles, resulting in a decrease in R_{et} (300Ω). In the P-L-Arg/GCE electrode (see Fig. 3A (curve b)), the R_{et} value of 900Ω is due to the positively charged P-L-Arg which promotes the electron transfer between the negatively charged $Fe(CN)_6^{3-/4-}$ and a strong electrostatic attraction with the negatively charged $Fe(CN)_6^{3-/4-}$ in the solution. Later, in the P-L-Arg/*f*-MWCNTs modified GCE electrode (see Fig. 3A (curve a)) the lowest R_{et} (300Ω) suggests kinetic and diffusion controlled processes because of P-L-Arg/GCE modified electrode, which almost shows a straight line. Further, GCE modification with GOx (see Fig. 3A (curve f)) gives a R_{et} of 2900Ω, the GOx is negatively charged and the negatively charged probe $Fe(CN)_6^{3-/4-}$ in the solution could be mainly because of the strong electrostatic repulsion. On the other hand, the GOx/P-L-Arg modified GCE exhibits a semicircle (R_{et} of 1800Ω) with little

increase in the diameter compared to that of GOx modified GCE. This proves that the GOx was immobilized on the P-L-Arg modified GCE electrode, which causes a small increase in the conductivity. Modification of the GCE in the electrode plays an important role in accelerating the transfer of electrons, thus decreasing the resistance in the GOx/P-L-Arg/*f*-MWCNTs Modified GCE electrode to $Fe(CN)_6^{3-/4-}$ (see Fig. 3A (curve d)). Additionally, the immobilization of GOx on the P-L-Arg/*f*-MWCNTs gives a lower R_{et} value = 1300Ω. Thus, the EIS results confirmed that the GOx was successfully immobilized on the surface of the P-L-Arg/*f*-MWCNTs and further hindered electron transfer on the electrochemical probe.

[Fig. 3]

3.2. Electrochemical characteristics and direct electrochemistry of GOx on the P-L-Arg/f-MWCNTs/GCE electrode

The electrochemistry of the GOx/P-L-Arg/*f*-MWCNTs/GCE modified electrodes can be studied using cyclic voltammetry as shown in Fig. 3B. In the pH 6.5 PBS, there was no current peak observed in the particular potential range of -0.2 to -0.8V for the bare GCE electrode (a), P-L-Arg/GCE (c), or Nafion/ P-L-Arg/*f*-MWCNTs/GCE (e). After combination with GOx, a pair of ill-defined and irreversible redox peaks could be observed for the GOx/P-L-Arg/GCE modified electrodes. The cathodic and anodic peak potentials were -0.404 and -0.339V. The formal potential (E°), calculated from the average value of the cathodic and anodic peak potentials was -0. 372V. This indicates the slow electron-transfer process as a consequence of the GOx. Furthermore, these results demonstrated that the modified film provided a biocompatible microenvironment for enzyme loading that retained the native bioactivity, although GOx/P-L-Arg/GCE was shown to be less stable. However, when the *f*-MWCNTs was introduced into the P-L-Arg film, the GOx/P-L-Arg/*f*-MWCNTs/GCE showed stable, well-defined and reversible

redox peaks at -0.360 V and -0.292 V, with a peak-to-peak separation of about 68 mV at a scan rate of 100mVs^{-1}, indicative of fast electron transfer. In addition, there was a remarkable increase in the current responses. The redox peaks remained almost unchanged after continuous 100 cycling, as can be seen in Fig. S2. Obviously, the response of Nafion/GOx/P-L-Arg/*f*-MWCNTs/GCE can be attributed to the redox of the electroactive centers of the immobilized GOx. Although a couple of symmetrical redox peaks for the FAD/$FADH_2$ also appeared, yet both the reduction and the oxidation peak currents for the GOx/P-L-Arg/GCE were much smaller than those of the Nafion/GOx/P-L-Arg/*f*-MWCNTs/GCE.The experimental results detailed above show that the background current of the P-L-Arg/*f*-MWCNTs/GCE (see Fig. 3B (d)) composite is higher than that of the P-L-Arg/GCE (see Fig. 3B (c)) or bare GCE (see Fig. 3B (a)), which are due to the participation of the loaded *f*-MWCNTs. The results suggested that the presence of *f*-MWCNTs on P-L-Arg and GCE surface had great improvement on the electrochemical response, which was partly due to excellent properties of *f*-MWCNTs such as good electrical conductivity, high chemical stability and high surface area. The higher currents in the cyclic voltammogram of the L-Arg/*f*-MWCNTs/GCE electrode show the high conducting nature and increased active surface area at L-Arg/*f*-MWCNTs/GCE. It is possible that the attaching of GOx to the surface of the P-L-Arg/*f*-MWCNTs/GCE offers more spatial freedom in terms of its orientation. Therefore, the present P-L-Arg/*f*-MWCNTs/GCE facilitates direct electron transfer between the heme sites in the immobilized GOx and the electrode surface.

The electrochemical behavior of the GOx/P-L-Arg/*f*-MWCNTs/GCE composite film modified GCE is studied at different scan rates; the PBS has a pH of 6.5, as shown in Fig. 4A. The peak to peak separation (ΔE_p) varies from 10 mV to 100 mV while the scan rate increases from 0.01Vs^{-1} to 0.1 Vs^{-1}. There is a significant increase in both the peak current (I_p) and ΔE_p

values with the increase of the scan rate. Moreover, both I_{pa} and I_{pc} increase linearly with the increasing scan rates, showing that the redox process of GOx at the modified electrode was a surface-controlled process. In addition, the surface coverage of the enzyme (Γ) at the modified electrode was calculated using the following equation: [45]

$$I_p = n^2F^2 vA\Gamma/4RT, \text{----------} (1)$$

Where n is the number of electrons involved; A (cm^2) is the surface area of the electrode; and v (Vs^{-1}) is the scan rate. The constants R, T and F represent their usual meanings, R=8.314 J $K^{-1}mol^{-1}$, T=298 K, and F=96485 C mol^{-1}, respectively. The surface coverage of the enzyme GOx is calculated using the slope of the plot between the scan rate and peak currents in the above equation, and found to be 1.76×10^{-10} mol cm^{-2}. The high value of Γ shows that the modified electrode accommodates high enzyme loading. The combination of the *f*-MWCNTs and P-L-Arg provides a large surface area for the immobilization of enzymes and as a result large amounts of enzymes were attached to the P-L-Arg/*f*-MWCNTs/GCE modified electrode. The amount of electroactive enzymes immobilized by the GOx/P-L-Arg/*f*-MWCNTs/GCE electrode is superior to the amount immobilized by the GOx/CdS modified electrode (1.54×10^{-11} mol cm^{-2}), [46] GOx/Au nano/carbon paste electrode (9.8×10^{-12} mol cm^{-2}), [47] or Nafion-CNTs-CdTe-GOx film (8.77×10^{-11} mol cm^{-2}). [48]

According to the equations of the Laviron model, the electrochemical parameters of the electrode reaction can be estimated by exploring the relationship between the peak current of the redox couples and scan rates ($n\Delta E_p$ >200mV): [49]

$$\log K_s=\alpha \log(1-\alpha) + (1-\alpha) \log\alpha - \log (RT/nFv) - \alpha (1-\alpha)nF\Delta E_p/2.3RT, \text{-------} (2)$$

Where α is the charge transfer coefficient with a value of 0.5 and the remaining parameters have the usual meanings as explained in equation (1). All the values were substituted into equation (2) and the apparent heterogeneous electron transfer rate constant (k_s) was calculated to be 5.16 s^{-1}. The high value of k_s indicates a faster electrode reaction due to the redox reaction at the GOx/P-L-Arg/*f*-MWCNTs film modified GCE. The k_s value of 5.16 s^{-1} for the GOx/P-L-Arg/*f*-MWCNT/GCE is comparatively larger than the values reported previously for the MWCNT chitosan (1.08 s^{-1}), [50] MWCNTs-CTAB (1.53 s^{-1}) modified electrodes, [51] boron-doped MWCNTs (1.56 s^{-1}), [52] GCNT/GOx/GAD (1.08 s^{-1}), [53] GC/CNT/Au/PDDA-GOx (1.01 s^{-1}), [54] or CNTs-poly (diallyldimethylammonium chloride) (PDDA) modified electrode (2.76 s^{-1}). [55] Hence it can be seen that the P-L-Arg/*f*-MWCNTs film provides an efficient platform for the immobilization of a large quantity of enzymes and also facilitates faster electron transfer reactions.

[Fig. 4]

The electrochemical behavior of the self-assembled GOx/P-L-Arg/*f*-MWCNTs/GCE should be pH dependent. In the range of pH 3-11, a pair of stable and well-defined redox peaks are exhibited. The redox reaction of GOx at the P-L-Arg/*f*-MWCNTs/GCE modified electrode features two-electrons coupled with two-proton reactions and can be expressed as follows in equation (3). [56,57]

$$GOx - FAD + 2e^- + 2H^+ \longrightarrow GOx - FADH_2. \quad (3)$$

Different pH studies were demonstrated using a PBS of pH 6.5 to find the nature of the redox coupling for various solution pH solutions. As shown in Fig. 4B, there is a negative shif in the formal potential, (Ec + Ea)/2 of the $FAD/FADH_2$ redox couple in GOx at the P-L-Arg/*f*-MWCNT/GCE modified electrode with increasing pH values, with a slope of 52.3 mV/pH in the

pH range of 3-11. This slope is reasonably close to the theoretical value of 58 mV/pH at 20 °C for a reversible two-electrons transfer coupled with two-proton transportation. This might be attributed to the special ion-exchange ability of the P-L-Arg/*f*-MWCNTs/GCE modified electrode .The P-L-Arg/*f*-MWCNTs/GCE modified electrode can exchange electrons and protons as well. The number of charges at the P-L-Arg/*f*-MWCNTs/GCE modified electrode surface varies with the pH, resulting in a different amount of exchanged protons.

3.3. Amperometric response of hydrogen peroxide biosensor

Hydrogen peroxide (H_2O_2) is an important chemical, which is widely used in the food, pharmaceutical, chemical and biochemical industries. In recent years, the fabrication and development of chemical sensors for H_2O_2 detection has become very important. Therefore, P-L-Arg/*f*-MWCNTs/GCE were employed as a sensing element to develop an electrochemical sensor for recognition of H_2O_2 using CV technique. Under the optimal experimental conditions, the electrochemical sensor shows remarkable response to the concentration changes of H_2O_2 (see Fig.S2). As seen, the I_{pc} currents increased linearly with increasing H_2O_2 concentrations. Therefore, H_2O_2 is effectively detected by reduction on the P-L-Arg/*f*-MWCNTs/GCE. Furthermore, the low I_{pc} potential of H_2O_2 (-0.4 V) is not affect by the oxidizable interfering species such as UA and AA which are the most important electroactive molecules which coexist with H_2O_2 in a biological system.[58] Thus, The P-L-Arg/*f*-MWCNTs/GCE electrode showed high catalytic response by addition of H_2O_2 which indicate that the P-L-Arg/*f*-MWCNTs/GCE is more sensitive for H_2O_2 compare with bare/GCE as shown in Fig.S2. When H_2O_2 was added into this system, it restrained the electrocatalytic reaction due to the non enzyme-catalyzed reaction as shown in the following equation:

P-L-Arg/*f*-MWCNTs

$$H_2O_2 + 2H^+ + 2e- \longrightarrow 2H_2O \quad (4)$$

On the other hand, the amperometric response of P-L-Arg/*f*-MWCNTs nanocomposites for successive addition of H_2O_2 was investigated in Fig.S3. The reduction current could achieve 95% of the steady-state current within 5s. The current response was enhanced as more H_2O_2 was added. This was ascribed to the fact that the P-L-Arg/*f*-MWCNTs nanocomposites on the rotating disc electrode surface efficiently accelerated the electron transfer. The inset of Fig. S3 displays the calibration plots of the biosensor for H_2O_2 determination.The linear range of the H_2O_2 detection was from 0.02 μM to 8 mM ($R^2 = 0.9916$) with a sensitivity of 36.16 μA cm^{-2} mM^{-1} at -0.4 V. The detection limit was estimated to be 50 nM based on the criterion of a signal-to-noise ratio of 3. further more, This experimental results indicated that the P-L-Arg/*f*-MWCNTs nanocomposites electrode offered high sensitivity and good stability for the detection of H_2O_2 at low potential in phosphate buffer solution. Thus, the P-L-Arg/*f*-MWCNTs could be used as an H_2O_2 sensor.

3.4. Electrocatalytic behaviors of the GOx/P-L-Arg/*f*-MWCNTs/GCE electrode towards glucose

Fig.5A showed the CVs of the GOx/P-L-Arg/*f*-MWCNTs nanocomposite modified GCE electrode in the presence of different concentrations of glucose in oxygen saturated PBS at the scan rate of 50 mV s^{-1}. The cathodic current at -0.45 V decreased linearly with the increase of glucose concentration. This result proves the excellent electrocatalytic ability of the GOx/P-L-Arg/*f*-MWCNTs modified GCE towards the enzymatic electro catalysis of glucose via the reduction of oxygen. The calibration curve corresponding to cyclic voltammetry response was

linear against the glucose concentration ranging from 0 to 10 mM (R^2=0.9935) with a sensitivity of 18.24 μA/mM^{-1} cm^{-2}. The detection limit was estimated to be 0.4 mM (S/N=3). It was well known that the normal range of blood glucose concentration was 4.4-6.6 mM and the diabetic glucose concentration was above 7.0 mM, which indicated that this biosensor was suitable for its practical application for the determination of human blood glucose concentration. Furthermore, The results revealed that GOx retained its specific enzyme activity at the P-L-Arg/*f*-MWCNTs surface without any denaturation. Highly biocompatible P-L-Arg film provides favorable microenvironment for GOx, allowing it to have direct electron transfer with the electrode surface through highly conductive *f*-MWCNTs networks.Therefore, we demonstrated the suitability of GOx-/P-L-Arg/*f*-MWCNTs modified GCE as a biosensor for the amperometric determination of glucose. The mechanism of reduction of dissolved oxygen and oxidation of glucose by GOx is explained in Equations (5). [45,59]

$$\text{Glucose} + \text{GOx (FAD)} \longrightarrow \text{Gluconolactone} + \text{GOx (FADH}_2\text{)}, \quad (5)$$

$$\text{GOx (FADH}_2\text{)} + O_2 \longrightarrow \text{GOx (FAD)} + H_2O_2, \quad (6)$$

$$O_2 + 4H^+ + 4e^- \longrightarrow 2H_2O. \quad (7)$$

[Fig. 5]

Fig.5B illustrates typical steady-state amperometric determination of glucose at GOx/P-L-Arg/*f*-MWCNTs rotating disc electrode upon successive addition of glucose into the air-saturated 0.05 M pH 7.0 PBS under the applied potential of -0.45 V.The sensor responds rapidly and approaches about 98% of its steady state currents within 5 s. Such fast response may be ascribed to the presence of P-L-Arg and *f*-MWCNTs in the nanocomposite. The presence of P-L-Arg and *f*-MWCNTs could increase the conductivity of P-L-Arg/*f*-MWCNTs namocomposite

and GOx in such matrix could quickly transfer electrons to electrodes. The insert to Fig. 5B shows a calibration plot between the added concentrations of glucose against the response current. Linear range spans the concentration of glucose from 4.0 μM to 6 mM (R^2=0.9918). The sensitivity of the biosensor is found to be 48.86 μA cm^{-2} mM^{-1}, its experimental detection limit is 0.1 μM at a signal-to-noise ratio of 3 for the GOx/P-L-Arg/*f*-MWCNTs sensor. We have summarized various glucose sensors in Table 1 with respect to the applied potential, the detection limit, the sensitivity and Km value. It can be seen that the proposed GOx/P-L-Arg/*f*-MWCNTs electrode shows a good performance than other glucose sensors sensors. The favorable attachment of GOx molecules with P-L-Arg/*f*-MWCNTs facilitates the better electrocatalytic performance of the glucose biosensor. The apparent Michaelis-Menten kinetic mechanism can be obtained using the Lineweaver-Burk equation: [60]

$$\frac{1}{i_{ss}} = \frac{K_m^{app}}{i_{max}} \frac{1}{C} + \frac{1}{i_{max}} \quad (8)$$

Here, I_{ss} is the catalytic current; i_{max} is the maximum current measured under saturated substrate conditions; $\boldsymbol{C}$ is the bulk concentration of the substrate; and K_m is the Michaelis-Menten constant. After substituting all the known values into the equation (8), the K_m value is calculated to be 2.2 mM. The smaller K_m value implies that the immobilized GOx possesses fabulous enzymatic activity and exhibits remarkable affinity for glucose in the GOx/P-L- Arg/*f*-MWCNTs nanocomposites matrix.

3.5. Determination of glucose in a serum sample

To illustrate the feasibility of the present biosensor based on the GOx/P-L-Arg/*f*-MWCNTs/GCE film for a practical usage as a glucose sensor, we tested samples of human plasma to determine their glucose concentration and compared the results to those obtained in the hospital by the spectrometric method. In this analysis, the real samples were diluted using a PBS of pH 6.5. The contents of glucose in the blood were then calculated from the calibration curve. The results are summarized in Table 2. It can be seen that the results are satisfactory and agree very closely with the hospital data. This indicates that the GOx/P-L-Arg/*f*-MWCNTs/GCE film is suitable for use in the proposed glucose biosensor and practical applications.

3.6. Reproducibility, stability, repeatability and precision of the Nafion/GOx/P-L-Arg/*f*-MWCNTs/GCE biosensor

The reproducibility is studied by recording CVs in a PBS of pH 6.5 at the scan rate of 50 mVs^{-1} following the addition of 1 mM concentrations of glucose. The sensor shows good reproducibility with an RSD of 3.2% for the five measurements. Similarly, the GOx-P-L-Arg/*f*-MWCNTs/GCE biosensor shows the acceptable repeatability with and RSD of 3.12% for 8 successful measurements. We examined the long-term storage stability of the GOx/P-L-Arg/*f*-

MWCNTs/GCE biosensor by testing the activity of the electrode with respect to storage time. The biosensor was stored at 4°C in a refrigerator. The performance towards glucose determination was monitored every day and the results compared with the initial performance. The results of the CV studies revealed that 95% of the initial response current were retained after 25 days of storage for the modified electrode.

4. Conclusions

In summary, the direct electrochemistry of GOx entrapped in P-L-Arg/*f*-MWCNTs films could provide a favorable microenvironment around the protein to retain the native structure and bioactivity of immobilized proteins. The biosensor has great capability for catalyzing the oxidation of glucose to H_2O_2 and can be used as an amperometric sensor for the determination of glucose. The P-L-Arg/*f*-MWCNTs/GCE exhibits a large surface area and good biocompatibility with improved conductivity for the redox activity of GOx. The P-L-Arg/*f*-MWCNTs/GCE modified electrode shows excellent electrocatalytic activity towards the reduction of H_2O_2 along with good stability and repeatability. The reason for this is that the P-L-Arg works as an electron conducting bridge between the prosthetic groups of the enzymes and the electrode surface and therefore can facilitate the electron transfer process.

Acknowledgement

The authors gratefully acknowledge the financial support received from the Ministry of Science and Technology, Taiwan (Republic of China).

References

[1] A. A. Karyakin, *Bioelectrochemistry*,2012,**88,**70-75.

[2] J. Wang, *Chem. Rev.* 2008,**108**,814-825.

[3] P. Si, P. Kannan, L. Guo, H. Son, D.H. Kim, *Biosens. Bioelectron*.2011,**26,**3845-4385.

[4] M. H. Asif, S. M. Ali, O. Nur, M. Willander, C. Brnnmark, P. Strlfors, U.H. Englund, *Biosens. Bioelectron*.2010,**25,**2205-2211.

[5] J. Wang, *Electroanalysis*,2011,**13**,983-988.

[6] X. L. Wang, Y. Zhang, C. C. Cheng, R. R. Dong and J. C. Hao, *Analyst*, 2011, **136**, 1753-1759.

[7] M. Pleitez, H. Lilienfeld-Toal and W. Mantele, *Spectrochim. Acta*, Part A,2011,**85**,61-65.

[8] L. Bahshi, R. Freeman, R. Gill and I. Willner, *Small*,2009,**5**,676-680.

[9] X. Y. Li, Y. L. Zhou, Z. Z. Zheng, X. L. Yue, Z. F. Dai, S. Q. Liu and Z. Y. Tang, *Langmuir*, 2009, **25**, 6580-6586.

[10] W. T. Wu, J. Shen, Y. X. Li, H. B. Zhu, P. Baneriee and S. Q. Zhou, *Biomaterials*, 2012, **33**, 7115-7125.

[11] Y. L. Wang, L. Liu, M. G. Li, S. D. Xu and F. Gao, *Biosens. Bioelectron*., 2011, **30**,107-111.

[12] G. Wang, K. Mantey, M. H. Nayfeh and S. T. Yau, *Appl. Phys. Lett*., 2006, **89**, 243901.

[13] G. Wang, S. T. Yau, K. Mantey and M. H. Nayfeh, *Opt. Commun*., 2008, **281**,1765-1770.

[14] O. Courjean, F. Gao and N. Mano, *Angew. Chem., Int. Ed*., 2009,**48**,5897.

[15] A. Heller, B. Feldman, *Chem. Rev*.2008,**108,**2482-2505.

[16] A. Riklin, E. Katz, I. Willner, A. Stocker, A.F. Buchmann, *Nature*,1995,**376,**672-675.

[17] D. Chen, G. Wang, J. Li, *J. Phys. Chem*. C,2007,**111,**2351-2367..

[18] C. Cai, J. Chen, *Anal. Biochem.,*2004,**332,**75-83.

[19]X. Kang, J. Wang, H. Wu, I.A. Aksay, J. Liu, Y. Lin, *Biosens. Bioelectron*.,2009,**25**,901-905.

[20] S. Liu, J. Tian, L. Wang, Y. Luo, W. Lu and X. Sun, *Biosens. Bioelectron* 2011, **26**, 4491-4496.

[21] A. Salimi, E. Sharifi, A. Noorbakhsh, S. Soltanian, *Biosens. Bioelectron*.,2007,**22,**3146-3153.

[22] G. Liu, M.N. Paddon-Row, J.J. Gooding, *Electrochem. Commun*.2007,**9,**2218-2223.

[23] X. Xiao, B. Zhou, L. Zhu, L. Xu, L. Tan, H. Tang, Y. Zhang, Q. Xie, S. Yao, *Sens.Actuators, B*,2012,**165**,126-132.

[24] C. Niu, E.K. Sichel, R. Hoch, D. Moy, H. Tennent, Applied Physics Letters,1997,**70,**1480.

[25] J.D. Zhang, M.L. Feng, H. Tachikawa, *Biosens. Bioelectron*.2007,**22**,3036-3041.

[26] Wang J. Carbon-nanotube based electrochemical biosensors:a review. *Electroanalysis*, 2005,**17**,7-14.

[27] B. Smith, K.Wepasnick, K. E. Schrote, H.H. Cho,W.P. Ball,D. H. Fairbrother,*Langmuir*, 2009, **25**, 9767-9776.

[28] K. A. Wepasnick, B. A. Smith, K. E. Schrote, H. K. Wilson,S. R. Diegelmann, D. H. Fairbrother,*Carbon*,2011,**49**, 24-36.

[29] T. A. Saleh, *Appl. Surf. Sci*.,2011, **257**,7746-7751.

[30] D. Yang, G. Guo, J. Hu, C. Wang, D. Jiang, *J. Mater. Chem*. 2008,**18**,350-354.

[31] F.C. Moraes, M.F. Cabral, L.H. Mascaro, S.A.S. Machado, *Sur. Sci.*, 2011,605,435-440.

[32] A. Liu, I. Honma, H. Zhou, *Biosens. Bioelectron*., 2007,**1**,74-80.

[33] T. Ramanathan, F.T. Fisher, R.S. Ruoff, L.C. Brinson, *Chem. Mater*., 2005,**17,**1290-1295.

[34] N.A. Kumar, A. Bund, B.G. Cho, K.T. Lim, Y.T. Jeong, *Nanotechnology*,2009,**20**,225-301.

[35] F. Zhang, S. Gu, Y. Ding, L. Zhoua, Z. Zhang, L. Li,*J. Electroanal. Chem.*,2013,**698**,25-30.

[36] L. Yamin, Y. Zhuo, J. Zhou, J. Liu, G. Song, K. Zhang, Y. Baoxian,*J. Electroanal. Chem.*, 2012,**687**,51-57.

[37] Q. Cao, H. Zhao, Y.M. Yang, Y.J. He, N. Ding, J. Wang, Z.J. Wu, K.X. Xiang, G.W. Wang, *Biosens. Bioelectron*.2011,**26,**3469-3474.

[38] Y. Li, Z. Ye, J. Zhou, J. Liu, G. Song, K. Zhang, B. Ye, *J. Electroanal. Chem.*, 2012,**687**,51-57.

[39] F.Y. Zhang, Z.H. Wang, Y.Z. Zhang, Z.X. Zheng, C.M. Wang, Y.L. Du, W.C. Ye, *Talanta*, 2012,**93,**320-325.

[40] P. Ayala, R. Arenal, M. Rummeli, A. Rubio,T. Pichler, *Carbon*,2010,**48,**575-586.

[41] B. P. Singh, Deepankar Singh, R. B. Mathur and T. L. Dhami, *Nanoscale Res Lett*., 2008,**3** 444-453.

[42] S.J. Bao, C. Li, J.F. Zang, X.Q. Cui, Y. Qiao, J. Guo, *Adv. Funct. Mater*.,2008,**18**,591-599.

[43]M.Guascito,D.Chirizzi,C.Malitesta,E.Mazzotta, *Analyst*,2011,**136**,164-173.

[44] K.Galhardo,R.Torresi,I.Susana,C.Torresi, *Electrochim. Acta*,2012,**73**,123-128.

[45] V. Mani, B. Devadas, S.M. Chen, *Biosens. Bioelectron*., 2013,**41**,309-315.

[46]Y. Huang, W. Zhang, H. Xiao, G. Li, *Biosens. Bioelectron*.,2005,**21**,817-821.

[47]S. Liu, H. Ju, *Biosens. Bioelectron*.,2003,**19,**177-183.

[48]Q. Liu, X. Lu, J. Li, X. Yao, J. Li, *Biosens. Bioelectron*., 2007,**22**,3203-3209.

[49] E. Laviron, *J. Electroanal. Chem*.,1979,**101,**19-28.

[50] X. Luo, A.Killard, M.Smyth, *Electroanalysis*,2006,**18,**1131-1134.

[51] A.Elie, C.Lei, R. Baughman, *Nanotechnology*,2002,**13,**559-564.

[52] C. Cai , *J. Chen. Anal Biochem.***,**2004,**332**,75-83.

[53] C. Deng, J. Chen, X. Chen, C. Xiao, L. Nie, S. Yao, *Biosens. Bioelectron*.,2008,**23,**1272-1277.

[54] A.Periasamy, Y.Chang, S.Chen, *Bioelectrochemistry*,2011,**80**,114-120.

[55] Y. Yao, K. Shiu, *Electroanalysis*,2008,**20**,1542-1548.

[56] D. Wen, Y. Liu, , G.C.Yang, S.J. Dong, *Electrochim. Acta*,2007,**52**,5312-5317.

[57]S.Palanisamy, C.Karuppiah, S.Chen, *Colloids Surf., B*,2014,**114,**164-169.

[58] S. Liu, B. Yu,T. Zhang,RSC Adv., 2014, 4, 544-548.

[59] B. Unnikrishnan, S. Palanisamy, S. Chen. *Biosens. Bioelectron*., 2013, **39**,70-75.

[60] H. Lineweaver, D. Burk, *J. Am. Chem. Soc*., 1934,**56**,658-666.

[61] Y. Oztekin, A. Ramanaviciene, Z. Yazicigil, A.O. Solak, A. Ramanavicius,*Biosens.*

Bioelectron., 2011,**26**,2541-2546.

[62] B. Liang, L. Fang, G. Yang, Y. Hu, X. Guo, X. Ye, *Biosens. Bioelectron*., 2013,**43**,131-136.

[63] H. Razmi, R. Mohammad-Rezaei, *Biosens. Bioelectron*., 2013,**41**,498-504.

[64] Y. Wang, L. Liu, M. Li, S. Xu, F. Gao, *Biosens. Bioelectron*., 2011, **30**, 107-111.

[65] J. Li, Z. Yang, Y. Tang, Y. Zhang, X. Hu, *Biosens. Bioelectron*., 2013, **41**, 698-703.

[66] Z.Nasri, E.Shams, *Electrochim. Acta*, 2013,**112**, 640-647.

[67] S. J. Bao, C. Li, J. F. Zang, X. Q. Cui, Y. Qiao, J. Guo, *Adv. Funct. Mater*., 2008,**18**,591-599

Fig. captions.

Schematic diagram of the preparation of the GOx/P-L-Arg/ *f*-MWCNTs/GCE modified electrode for use in glucose biosensors.

Fig.1. (A) XPS spectra of P-L-Arg/ *f*-MWCNTs films. (B) C1s of P-L-Arg/ *f*-MWCNTs films (C) N 1s of P-L-Arg/ *f*-MWCNTs films (D) FTIR spectra of the: (a) *f*-MWCNTs; (b) P-L-Arg/*f*-MWCNTs , SEM images of (E) *f*-MWCNTs. Insert image shows the EDX spectra of *f*-MWCNTs films; (F) P-L-Arg/*f*-MWCNTs. Insert image shows the EDX spectra of P-L-Arg/*f*-MWCNTs films.

Fig. 2. SEM images of (A) GOx /P-L-Arg/*f*-MWCNTs. AFM images of (B) GOx /P-L-Arg/ *f*-MWCNTs. (C) FTIR spectra of the (a) GOx, (b) GOx/P-L-Arg, and (c) GOx/P-L-Arg/ *f*-MWCNTs. and (D) UV-Vis spectra of the (a) native GOx, (b) GOx/*f*-MWCNTs,(c) GOx/P-L-Arg, and (d) GOx/P-L-Arg/*f*-MWCNTs modified electrode.

Fig. 3. (A) EIS results for different electrodes in the 5mM $[Fe(CN)_6]^{4-/3-}$ containing 0.05 M PBS buffer solution: (a) P-L-Arg/*f*-MWCNTs/GCE; (b) P-L-Arg/GCE electrode; (c) Bare GCE electrode; (d) GOx/P-L-Arg/ *f*-MWCNTs /GCE electrode; (e) GOx/P-L-Arg/GCE electrode; (f) GOx/GCE electrode. Inset: Randles equivalent circuit model. (B) Cyclic voltammograms for the (a) bare GCE electrode; (b) GOx/P-L-Arg/GCE electrode; (c) P-L-Arg/GCE electrode; (d) P-L-Arg/ *f*-MWCNTs /GCE; and (e) GOx/P-L-Arg/ *f*-MWCNTs / modified GCE in N_2-saturated PBS (0.05 M, 6.5) at a scan rate of 100 mV s^{-1}.

Fig. 4. (A) CVs of GOx/P-L-Arg/ *f*-MWCNTs modified GCE in an N_2-saturated PBS (0.05 M, pH6.5) at different scan rates of: 10, 20, 30, 40, 50, 60, 70, 80, 90 and 100 mV s^{-1}. Inset: plot of the anodic and cathodic peak currents vs. scan rates. (B) CVs of the GOx/P-L-Arg/ *f*-MWCNTs modified GCE in an N_2-saturated PBS (0.05 M, pH6.5) with different pH values of: 3, 5, 7, 9, and 11. Scan rate: 50 mV s^{-1}. Inset: plot of the formal potential vs. pH value.

Fig.5. (A) CVs of GOx/P-L-Arg/ *f*-MWCNTs modified GCE to glucose with various concentrations of (a-k): 0 to 10 mM in O_2-saturated PBS (0.05 M, pH 6.5). (B) Amperometric response of the GOx/P-L-Arg/ *f*-MWCNTs rotating modified electrode for successive additions of glucose in the O_2-saturated PBS (0.05 M, pH 6.5) at an applied potential of -0.45 V. Inset: shows the calibration curve for glucose obtained by the biosensor.

Fig.

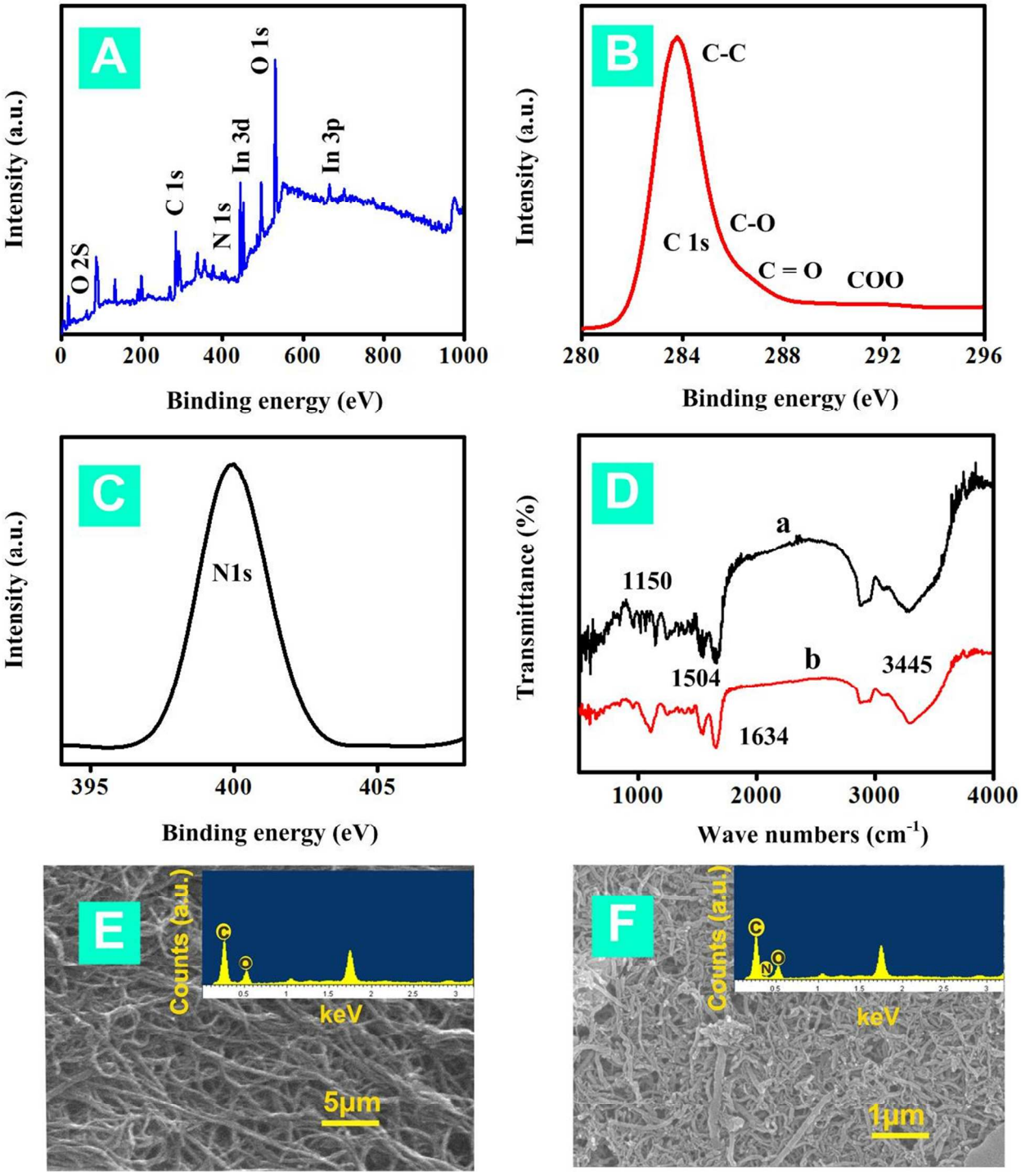

Fig. 1

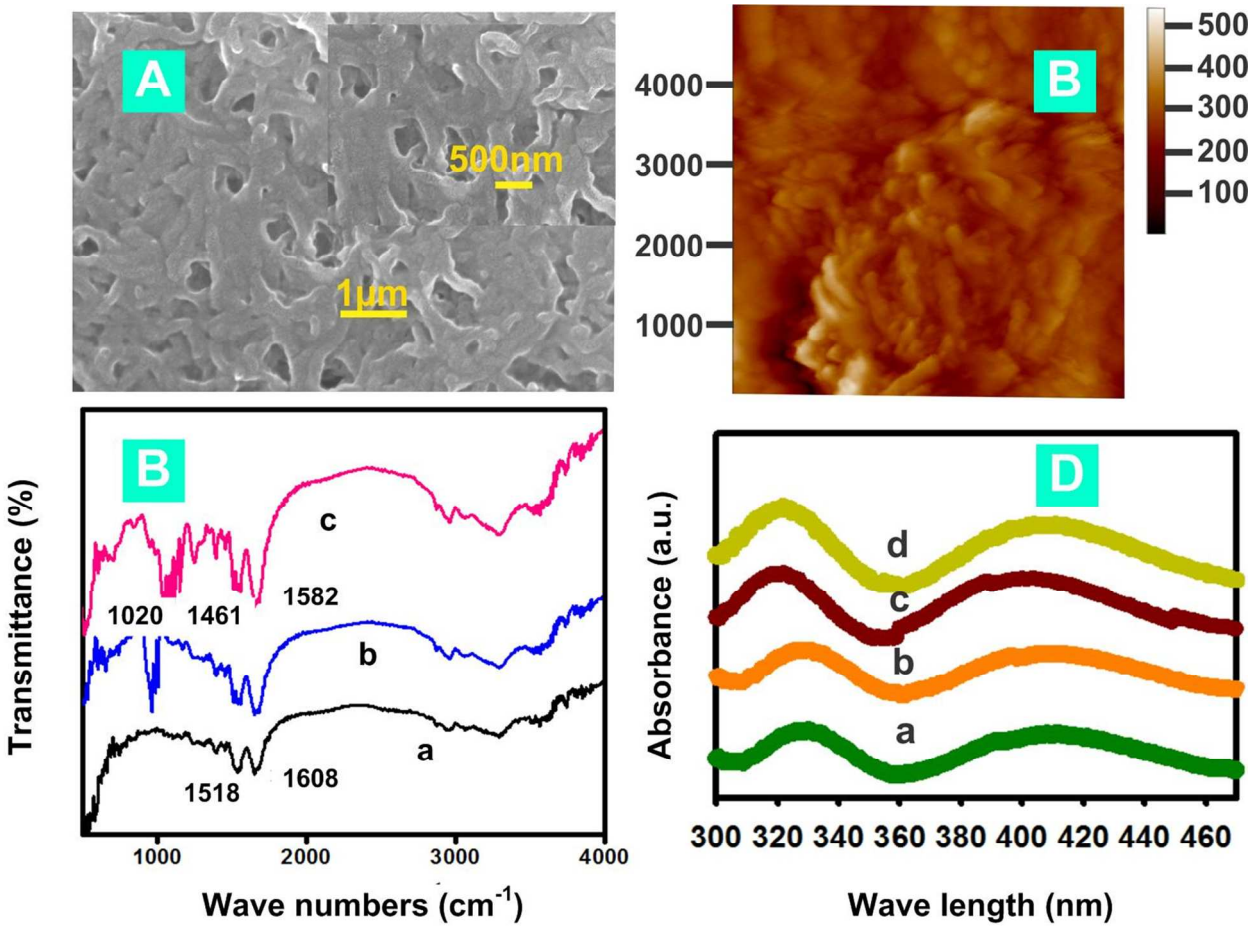

Fig. 3

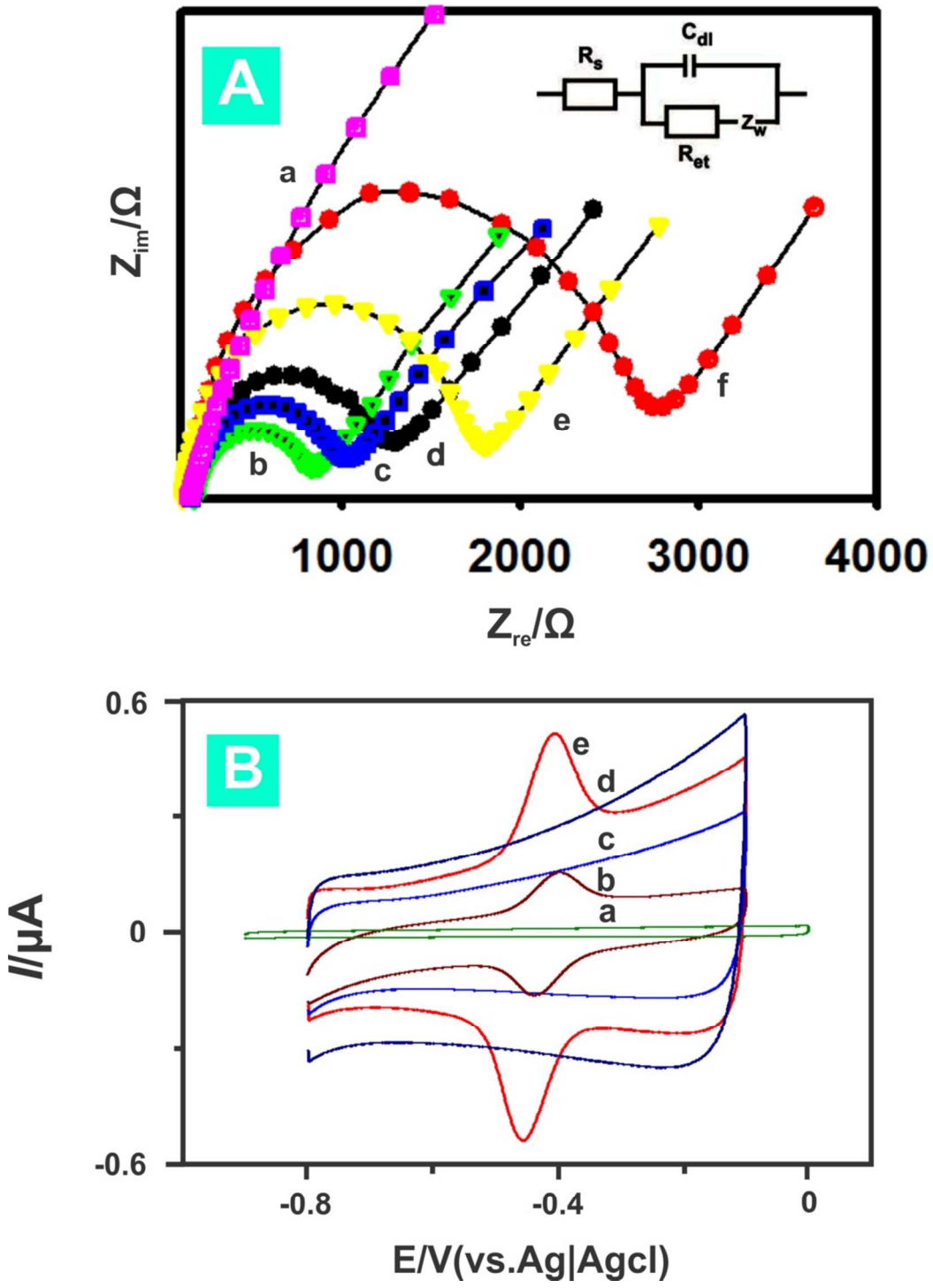

Fig. 3

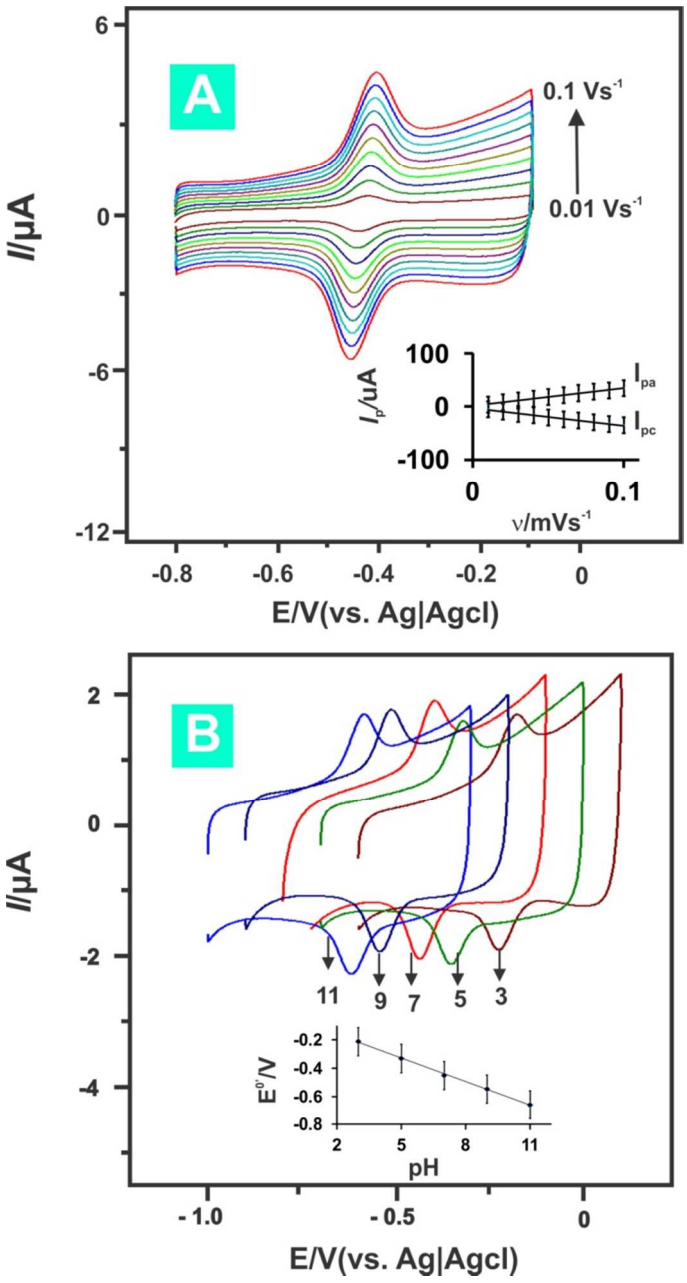

Fig. 4

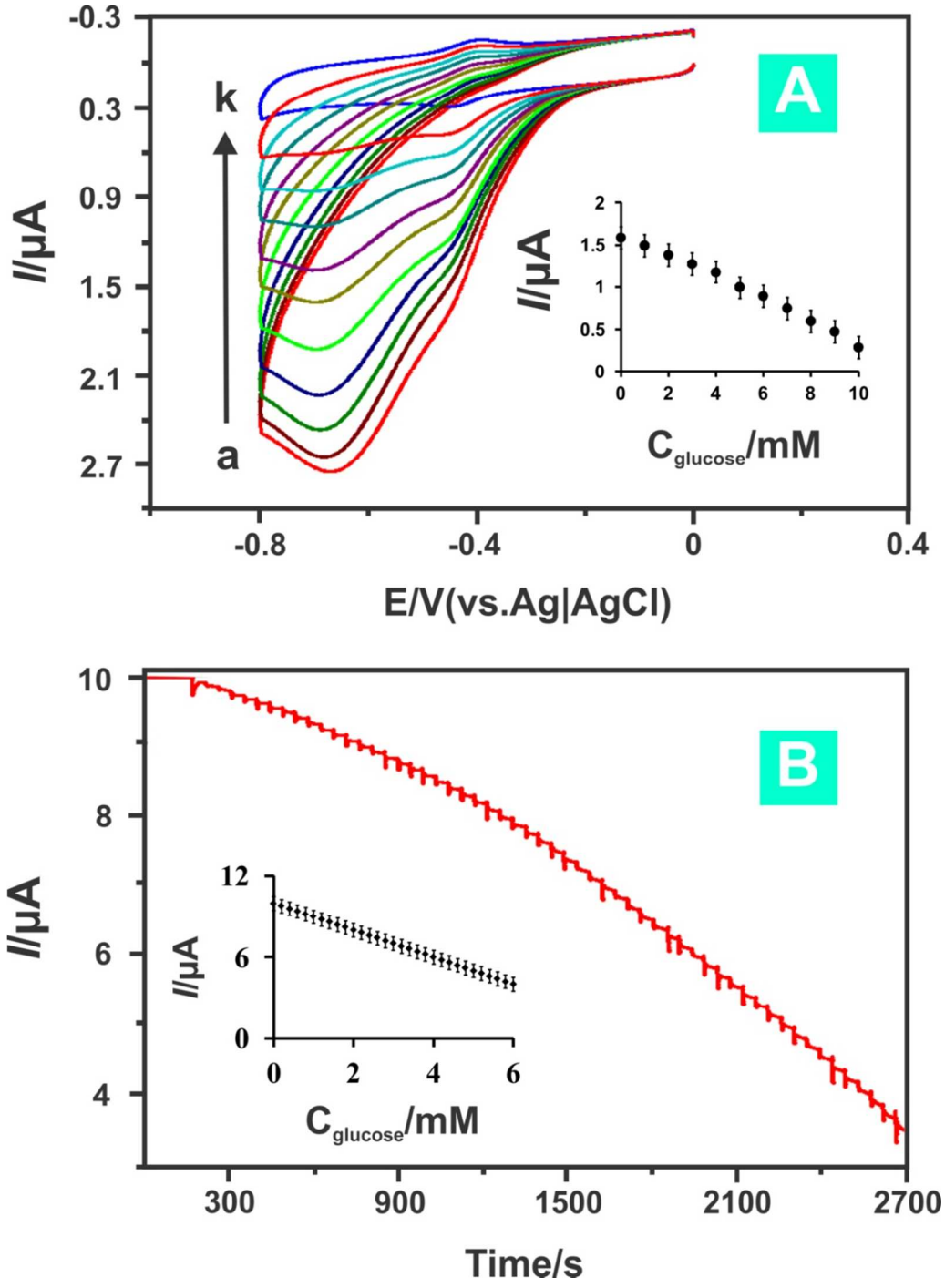

Fig. 5

Table 1

Comparison of analytical performance of different GOx based glucose sensors for determination of glucose.

Electrode	Applied potential (V)	Linear range (mM)	LOD (μM)	K_M(mM)	Ref
Electrochemically reduced graphene oxide- multiwalled carbon nanotubes hybrid modified GCE electrode	+0.35	0.01-6.5	4.7	-	[45]
GOx/ poly-1,10-phenanthroline modified GCE electrode	+0.20	0.05-48	50	0.64	[61]
GOx/ electrochemically reduced carboxyl graphene modified GCE electrode	-0.46	2-18	20	-	[62]
GOx- Graphene quantum dots modified carbon ceramic electrode	-0.42	0.005-1.270	1.73	0.76	[63]
Nafion/ GOx /Ag-Polydopamine @CNT modified GCE electrode	-0.50	0.05-1.1	17	5.46	[64]
MWCNTs-SnS_2 modified GCE electrode	-0.43	0.02-1.95	4	2.71	[65]
GOx/4-aminophenyl modified GCE electrode	-0.45	0.05-4.5	10	2.95	[66]

TiO_2/ GOx /Nafion–modified GCE electrode	-0.45	0.15-1.2	-	-	[67]
GOx/P-L-Arg/*f*-MWCNTs modified GCE electrode	-0.45	0.004-6	0.1	2.2	This work

Table 2

Analysis of glucose in human blood samples by the GOx/P-L-Arg/*f*-MWCNTs modified GCE

Sample	Added (μM)	Sample Found (μM)	R.S.D (%)	Recovery rate (%)
1	0	530.5	3.2	-
2	50	582.2	2.9	104.4
3	500	1016.5	2.7	99.6